HHS Public Access

Author manuscript

Toxicol Pathol. Author manuscript; available in PMC 2017 April 01.

Published in final edited form as:

Toxicol Pathol. 2016 April ; 44(3): 373–381. doi:10.1177/0192623315622303.

Computed Tomography and Magnetic Resonance Imaging for Longitudinal Characterization of Lung Structure Changes in a Yucatan Miniature Pig Silicosis Model

Emily Hammond[1,2], **John D. Newell Jr.**[1,2], **Samantha K.N. Dilger**[1,2], **Nicholas Stoyles**[1], **John Morgan**[1], **Jered P. Sieren**[1], **Daniel R. Thedens**[1], **Eric A. Hoffman**[1,2], **David K. Meyerholz**[3], and **Jessica C. Sieren**[1,2]

[1]Department of Radiology, University of Iowa, Iowa City, Iowa

[2]Department of Biomedical Engineering, University of Iowa, Iowa City, Iowa

[3]Department of Pathology, University of Iowa, Iowa City, Iowa

Abstract

Medical imaging is a rapidly advancing field enabling the repeated, non-invasive assessment of physiological structure and function. These beneficial characteristics can supplement studies in swine by mirroring the clinical functions of detection, diagnosis, and monitoring in humans. In addition, swine may serve as a human surrogate, facilitating the development and comparison of new imaging protocols for translation to humans. This study presents methods for pulmonary imaging developed for monitoring pulmonary disease initiation and progression in a pig exposure model with CT and MRI. In particular, a focus was placed on systematic processes, including positioning, image acquisition, and structured reporting to monitor longitudinal change. The image-based monitoring procedure was applied to six Yucatan miniature pigs. A subset of animals (n = 3) were injected with crystalline silica into the apical bronchial tree to induce silicosis. The methodology provided longitudinal monitoring and evidence of progressive lung disease while simultaneously allowing for a cross-modality comparative study highlighting the practical application of medical image data collection in swine. The integration of multi-modality imaging with structured reporting allows for cross-comparison of modalities, refinement of CT and MRI protocols, and consistently monitors potential areas of interest for guided biopsy and/or necropsy.

Keywords

Computed tomography (CT); magnetic resonance imaging (MRI); longitudinal imaging; structured reporting; pig models; silicosis; medical imaging

Introduction

Medical imaging is a rapidly advancing field enabling the repeated, non-invasive assessment of physiologic structure and function. As a clinical imaging modality, computed tomography

Corresponding author information: Jessica C. Sieren, University of Iowa, 200 Hawkins Drive, Iowa City, IA 52242, (319)356-1407, jessica-sieren@uiowa.edu.

(CT) has a fast acquisition time, moderate cost, and superior structural resolution while magnetic resonance imaging (MRI) involves no ionizing radiation and has excellent soft tissue contrast. These modalities provide the opportunity to non-invasively characterize and compare progressive changes in pigs that can result from an intervention, exposure, or genetic manipulation. Longitudinal monitoring within the same animal can provide valuable information about the etiology of disease while also keeping the number of animals needed for a study to a minimum.

Animal models have been relied upon in medical research to advance biomedical and translational research for humans. Specifically, pig models can serve as a valuable human surrogate in imaging studies due to their similar anatomy, physiology, life-span, and size to humans (Swindle *et al.*, 2012, Svendsen, 2006). This allows for testing and validation of novel imaging methods on clinical imaging systems with direct comparison between multiple modalities, a feat that is challenging to accomplish in humans. For example, the pig lung anatomy is comparable to human structure, with similar lung volumes, airway dimensions and cardio-pulmonary rates; facilitating investigations of lung function (Kotoulas *et al.*, 2014), novel bronchoscopy techniques (Henne *et al.*, 2015, Tan *et al.*, 2012) and novel medical imaging methods (O'Connell *et al.*, 2015). Recently, genetically modified pig models have been developed of cancer and cystic fibrosis in which medical imaging has been used to provide valuable in-vivo insight (Sieren *et al.*, 2014a, Rogers *et al.*, 2008b, Rogers *et al.*, 2008a). Focus on longitudinal pulmonary assessment is of interest for these genetically modified models as well as for toxicological exposure models in pigs.

In this paper we outline the methods used for multi-modality, longitudinal image acquisition in a pig model of silicosis. Silicosis is a pneumoconiosis caused by crystalline silica particles in the lung. In humans, inhaled crystalline silica causes pulmonary inflammation, progressive fibrosis, airway wall thickening, and nodules. These conditions cause structural changes in the lung that can be observed through medical imaging (Mosiewicz *et al.*, 2004, Matsumoto *et al.*, 1998). We apply and evaluate the ability of these imaging techniques to track disease development in a pig model of silicosis, presenting a systematic approach for comparing the sensitivity of CT to MR for pulmonary assessment.

Materials and Methods

Model development

Six female Yucatan miniature swine were imaged for a total of 6 screening time points beginning at one year of age, as displayed in Table 1. All animals were heterozygotes with genetic modification of a common tumor suppressor gene ($TP53^{R167H/+}$). To induce silicosis in the lungs, the cohort was divided into a control (n=3) and exposure (n=3) cohort, with instillation of crystalline silica in the exposure cohort. Medium grain quartz foundry sand was ground to micron-sized (<4μm) dust using a ball mill (Retch, Inc., MM-400). Samples of 250 mg were weighed into clean borosilicate glass vials into which 5 mL of sterile 0.9% saline was pipetted. Samples were vortexed prior to loading into a syringe for instillation in a targeted region of the lungs. The silica was delivered to the right cranial lobe through the right apical bronchus via a bronchoscopic guided catheter, flushed with 2 mL saline and placement confirmed via CT imaging (Figure 1A). All animals were housed in the

Association for Assessment and Accreditation of Laboratory Animal Care (AAALAC)-accredited facilities and the experimental procedures approved by the Institutional Animal Care and Use Committee (IACUC).

Animal Preparation

All procedures were performed under anesthesia, induced with an intramuscular injection mixture of telazol (2.2 mg/kg), ketamine (1.1 mg/kg), and xylazine (1.1 mg/kg), and maintained with 3 – 5% isoflurane. All swine were mechanically ventilated through tracheal intubation with a balloon cuffed, 7 mm – 8 mm diameter endotracheal tube. Ventilation was performed with a 5 cm H_2O positive end expiratory pressure (PEEP) and an approximate tidal volume of 10 mL/kg using an MRI compatible, large animal anesthesia machine (DRE Premier XP, Louisville, KY). Enforced breath holds were used to prevent respiratory motion through short imaging acquisition protocols, achieved by suspending mechanical ventilation with a 20cm H_2O PEEP bi-directional flow guard (ACCU-PEEP, Vital Signs, Nashvile, TN). The ventilation protocol used a respiratory rate of 10–16 breaths/minute to maintain an end-tidal carbon dioxide pressure (ET-CO_2) between 35 and 45 mmHg and a blood oxygen saturation pressure (SpO_2) of 100%. Peripheral intravenous access was obtained via ear vein cannula (20 Gauge) for the administration of contrast and was maintained with heparinized saline (3–5 mL, 500 units/L) flushes.

Animals were placed supine in a positioning unit designed to maintain reproducible positioning during imaging (Hammond *et al.*, 2015). Physiologic monitoring was maintained through the duration of each animal imaging study, in CT with a Phillips physiologic monitor (Intellivue MP90, Phillips Healthcare, Best, The Netherlands), in transit with a portable physiologic monitor (Propac Encore, Welch Allyn Inc., Skaneateles Falls, NY), and in MRI with an MRI compatible physiologic monitor (Invivo MAGNITUDE:3150M, Medeco, Boise, ID).

Imaging Protocols

The strengths and weaknesses of CT and MRI for longitudinal lung disease assessment were evaluated in this model. CT was chosen for fast acquisition, high resolution, and quantitative imaging capabilities. Although MRI is not typically used clinically for pulmonary imaging, it was selected in this study as an alternative modality that does not require ionizing radiation, which is advantageous for longitudinal screening.

Chest CT scans were obtained with a 128-multidetector dual-source scanner (Somatom Definition Flash, Siemens Healthcare, Erlangen, Germany) to assess lung density and anatomical detail (210mAs and 120kV, a rotation time of 0.5 second, pitch of 1 and, a CTDIvol of 14.2mGy). No resultant effects were observed from this exposure, which is slightly higher than a standard clinical high resolution chest protocol and less than a CT angiography exam. Scans were acquired at an inspiratory breath-hold of 20 cmH_2O following 2 minutes of pulmonary recruitment at an equivalent PEEP. Mouth pressure was monitored with in-house LabVIEW software (National Instruments, Austin, TX) to confirm consistent inspiratory breath-holds during imaging. Reconstructions were performed with a

B35f Siemens kernel at slice thicknesses of 3 mm and 0.75 mm with 0.75 mm isotropic in-plane resolutions.

Chest MRI scans were acquired with a 3-Tesla MRI system (TIM Trio 3T, Siemens Healthcare, Erlangen, Germany) with standard surface coils. Turbo spin echo T2-weighted scans (TR of 5280 ms, TE of 156 ms, flip angle of 120°, and echo train length of 109) acquired in the axial and coronal planes were used to assess areas of increased fluid content, such as tumor development or inflammation. Five mm slice thicknesses were acquired with 1.4 mm × 1.8 mm and 1.5 mm × 2.0 mm in-plane resolution for the axial and coronal scans respectively. Respiratory gating was accomplished during this MRI sequence by using navigator echoes to eliminate respiratory induced motion artifacts. An additional post-contrast 3D single breath hold T1-weighted VIBE thoracic MRI scan (TR of 4.3 ms, TE of 1.92 ms, flip angle of 12°) was acquired post intravenous administration of 0.2 mL/kg gadolinium (Magnevist, Berlex Inc, Wayne, NJ) for increased anatomical detail in the lungs. In-plane resolutions of 1 mm × 1.8 mm were acquired at slice thicknesses of 3 mm. Breath-holds at an inspiratory pressure of 20 cm H_2O were used to reduce motion artifact for all VIBE scans.

Data Analysis

The completion of each screening time point using the above imaging protocol resulted in one CT scan and three MRI scans per subject. Comprehensive structured reports were developed for each modality, modeled after the Radiological Society of North America (RSNA) radiology reporting initiative (Kahn Jr *et al.*, 2009), to provide consistent and complete visual interpretation of the lungs and surrounding anatomies. Each structured report included the assessment of the diagnostic quality of the scan and targeted anatomic structures of interest. The anatomic structures of interest included the large airways, pleura, heart and pericardium, mediastinum and hila, chest wall and lower neck, vessels, and bones. Within the lungs, a total of eleven conditions were prompted for within each lobe of the lungs. These included consolidation, bronchiectasis, atelectasis, bronchial wall thickening, ground glass opacities, linear opacities, nodules, emphysema, cysts, reticular abnormalities and honeycombing. A subset of screening time points were analyzed using the structure reports to assess the agreement between the two imaging modalities with CT considered the gold standard for lung imaging. To minimize reader bias, scans were randomized by subject and time point within each modality resulting in pseudo time points read in one week intervals by a board certified chest radiologist (Author: J.D.N.). Structured reports were defined for each modality, subject, and screening time point and were matched with the corresponding randomized set. The T2 weighted thoracic images and the T1 weighted thoracic images were read in combination for the MRI structured reporting results. For each detected condition within a lobe, the number of incidences where both CT and MRI resulted in a congruent finding (presence and absence of the condition), divided by the total number of imaging time points was used to calculate the percent agreement.

Quantitative analysis of the CT data focused on the right cranial lobe of the lung to assess disease progression in the airways and surrounding lung parenchyma related to the silica exposure. Parenchymal analysis was performed with in-house software (PASS: Pulmonary

Analysis Software Suite) (Guo *et al.*, 2008). A three dimensional region of interest (ROI) was placed in the right cranial lobe for each CT dataset, and the mean CT density in that region was calculated (Figure 2A). To account for the variation in lung volume across and within subjects, density measures were normalized to the mean density of the entire lung. The apical bronchus and corresponding airway tree were automatically segmented from the chest CT scan using the Apollo quantitative lung imaging software (VIDA Diagnostics, Coralville, IA) (Figure 2B). The wall area fraction (wall area as a percent of the total airway area) was measured and used to assess change in the airways between the exposure and control cohorts.

Results

Screening time points required an average of 2 hours (SD 22 minutes) per subject, with average times of 40 minutes required for preparation, 45 minutes for imaging (15 CT, 30 MRI) with the majority of time required for positioning the animal in both modalities, and 35 minutes for recovery from anesthesia. All acquired scans were completed with excellent diagnostic image quality and minimal artifacts. For all CT scans, consistent inspiratory breath holds were achieved with an average 19.55 cm H_2O (SD 0.98).

Structured report results were tabulated and the percent agreement between modalities was tabulated (Table 2). There was 72% overall agreement in the type and location of pulmonary findings between the two modalities. In comparison, MRI proved useful in the detection of consolidation, bronchiectasis, atelectasis, and bronchial wall thickening with a level of agreement of 75% or above. At only 55% agreement, MRI systematically over estimated ground glass opacities in the lungs, particularly in the cranial and caudal lung lobes (Figure 3). In addition, MRI underestimated linear opacities (48%); mainly due to poor congruency in the lower lobes (17%) when MRI was compared to CT. With respect to lobar location in the lungs, the cranial lobes showed higher agreement (67%, 75%) than the lower lobes (58%, 51%) with the right middle (83%) and accessory (98%) lobe showing the greatest agreement; however, minimal findings occurred in the right middle and accessory lobes with both modalities.

The effects of silica instillation on the right cranial lobe in the exposure cohort generated new findings during serial imaging of this cohort: including ground glass opacities and the identification of multiple small nodules (2–3 mm) at 21 months in subject 4 (Figure 1). Via the structured reporting mechanism, the cranial lobes in both exposure and control animals had a high number of reported findings, with multiple minor transient changes reported. Quantitative CT based density and airway measures were obtained to objectively compare the severity and progression of structural changes in the exposure versus the control cohorts (Figure 2). CT attenuation is expressed in Hounsfield Units (HU) and is representative of tissue density, with water represented as 0 HU and air as −1000 HU. Normal mean lung CT attenuation values are reported to be −861 (SD 14) HU for men and −838 (SD 21) HU for women (Zach *et al.*, 2012). Over the course of the study the CT assessed lung density was very stable in the control group, as reflected in the minimal (±1%) percent change from baseline for this cohort, shown in Figure 2C. Silica exposure was performed at 14 months of age and confirmed via a 15% increase in mean CT lung attenuation in the targeted right

cranial lung lobe of the exposure group. This immediate increase in lung density was caused by fluid deposition in this target region (saline suspension and flush). At subsequent time points, CT assessed lung attenuation remained elevated from baseline for exposure animals compared to controls, ranging from an increase of 2% at 16 months to an increase of 4.5% at 36 months (Figure 2C). While subtle, this quantitative assessment reflects a progressive increase in lung density in the exposed region of the lung compared to the highly stable mean lung density in the control cohort. For the quantitative assessment of CT based airway measures, the wall area fraction was determined by dividing the airway wall area by the outer (total) airway area for each target airway branch. Measures acquired at 15 months post exposure (cohort 27 months of age) were compared to pre-exposure, baseline measures (cohort 12 months of age) to observe changes over time (Figure 2D). Here, evidence of airway wall thickening was observed in the cranial lobe segmental airways (RB1-5 and RB1-6) in the exposure group but not in the control group.

Pathological confirmation of silica deposits with corresponding fibrosis in the upper right lung (Figure 1) was obtained for subject 4 at 36 months of age (Figure 4). Necropsy occurred immediately following the final imaging time point with CT. Prosection of the lung was guided by the previously acquired MRI and CT images through three plane viewing and volume rendering to gauge correspondence between and within structures. The remaining two *TP53*$^{R167H/+}$ pigs exposed to crystalline silica demonstrate similar evidence of disease response with imaging and continue to be longitudinally monitored for disease progression.

Discussion

This study presents a method for non-invasively characterizing lung disease development in a pig model exposed to crystalline silica using CT and MRI. A pulmonary structured reporting method was developed to record pertinent information useful in the systematic, longitudinal phenotyping of pig models. With respect to imaging modalities, CT was selected for its fast acquisition of high resolution volumetric data, broad applicability, and wide availability in the clinical imaging field. MRI provided a strong complement with the lack of ionizing radiation making it ideal for longitudinal acquisition. This study shows that pig models can be used for controlled longitudinal studies directly comparing CT and MRI protocols that is not easily accomplished with humans and with direct translatability not found with small animals.

The developed thoracic structured reporting method focused on conditions noted in the lungs and provided a comparison between MRI and CT for lung disease screening using CT as the gold standard. Predictably, CT was superior over MRI in the detection of fine structural details, such as linear opacities. Comparatively, MRI was shown to be reliable in the detection of bronchiectasis, atelectasis, and bronchial wall thickening. However, the results indicated a large disagreement in the incidence of ground glass detected in MRI compared to CT. It was inferred that the presence of these ground glass abnormalities observed in the T1 post-contrast VIBE scans were artifacts which may be due to cardiac motion and/or the presence of contrast. In addition, it is possible these were real transient findings related to the fact that the MRI scans were obtained after the CT acquisitions. It follows that the animal had been on the ventilator longer so atelectasis and increased

secretions may have been present, specifically in the lower lobes despite lung recruitment maneuvers. We did not acquire ground truth pathology confirmation for the ground glass opacities detected with MRI. While the desired diagnostic quality was still attained in a majority of the scans with the management of respiratory motion, improved quality may occur with the use of cardiac gating and increased frequency of pulmonary recruitment. Due to these factors, routine imaging with CT is preferred for the early structural assessment of silicosis progression in pigs. Later stage disease may be adequately captured using MRI.

An additional advantage of CT data acquisition in this study was the ability to quantitatively assess the lung for density and airway structural changes over time using CT analysis software developed for human pulmonary assessment. The structural reporting mechanism aided in the comparison of findings between modalities and also assisted in distinguishing transient from persistent structural changes within a modality. However, the structured report did not capture the severity of a finding in a particular lobe and an approximately equal number of findings were reported in the right cranial lobes of exposure and control animals. Objective characterization of differences between the cohorts across time was achieved using quantitative CT image analysis of lung density and airway wall structure. Having established these methodologies, these findings support further exploration of these quantitative measures in a larger cohort to validate these biomarkers for the assessment of silicosis in pigs.

Incorporating medical imaging surveillance has proven to be a useful tool for pathological analysis of pig models. Imaging modalities can screen large volumes of tissue more effectively and efficiently than can be done at a typical necropsy. We have previously used whole body CT and MRI monitoring to identify tumor formation in a Li-Fraumeni *TP53*$^{R167H/R167H}$ cancer pig model (Sieren *et al.*, 2014a). Similar to tracking silicosis formation, detection of tumors via non-invasive medical imaging aided in the timing of necropsy and guidance of tissue collection for histopathological examination. In these cases, volume rendering is advantageous, specifically using CT due to the acquisition of isotropic voxels providing finer detail. Once regions of interest are identified they can be spatially targeted by their distance as precisely as 1 mm from selected anatomic landmarks, similar to the way imaging can guide surgeons during an operation (Ganz, 2005). Thus, imaging modalities complement and improve pathological examination and assessment of pig models. Overall, the imaging methods presented here have been developed with a focus on pulmonary assessment; however, this work provides a platform methodology on which variations in targeted organ imaging and reporting strategies may be developed as needed.

Due to their comparable size, the use of large animals has been previously reported for the development and translation of CT protocols to aid in the quantitative CT characterization of human emphysema (Won *et al.*, 2003, Alford *et al.*, 2010, Dakin *et al.*, 2008). Furthermore, pig models have similar metabolic activity and lifespan providing a more robust surrogate for targeted therapies developed in large animal models for subsequent translation to humans (Ellinwood and Clay, 2009, Bode *et al.*, 2010). The imaging protocols for this study were chosen to parallel clinical protocols with an emphasis on lung structure assessment. Data acquisition was facilitated by the availability of dedicated research CT and MRI scanners and technologists at our institution. Recent upgrade of our dedicated research CT

scanner (Somatom Force, Siemens Healthcare, Erlangen, Germany) will allow future studies to incorporate advanced radiation dose reduction methods, including more efficient x-ray detectors and more advanced iterative reconstruction algorithms, while maintaining comparable quality image data (Sieren *et al.*, 2014b, Mobberley *et al.*, 2013). In this study the high resolution, quantitative CT data was superior compared to the acquired structural MRI protocols in capturing early evidence of silicosis in a porcine model. It is important to note that our MRI protocols were optimized within the limitations of available MRI scanner (3T vs. 1.5T), coils, and software. Future application of ultra-short TE sequences on our 3T MRI system could further enhance lung structure assessment of MRI (Johnson *et al.*, 2013, Bell *et al.*, 2015). We can now use the developed structured reporting method and comparative analysis to assess performance of these methods. In addition, MRI can be advantageous for lung function assessment when incorporating hyperpolarized and/or inert fluorinated gas MRI, which will be future areas of development in this model (Fain *et al.*, 2007, Couch *et al.*, 2014).

To capture and track longitudinal changes in pulmonary structure due to disease development using medical imaging, we selected to expose a subset of $TP53^{R167H/+}$ pigs to crystalline silica. Silica exposure was selected for this study due to the progressive nature of silicosis formation that would provide an ideal model in which to compare longitudinal chest imaging techniques. In addition, crystalline silica is a carcinogen associated with lung cancer based on the study of occupational exposure (Rice *et al.*, 2001, Checkoway *et al.*, 1999, Cherry *et al.*, 1998) and supported by work in animals (Muhle *et al.*, 1995, Saffiotti, 1991). TP53 plays a vital role in cancer prevention through activation of DNA repair proteins, halting the cell cycle such that DNA repair proteins have time to complete reparation, and are able to initiate apoptosis in the case of DNA repair failure (Levine and Oren, 2009). We have previously demonstrated that $TP53^{R167H/R167H}$ pigs develop cancer (including lymphoma, osteosarcoma and Wilms tumor) but have detected no cases of lung cancer in the $TP53^{R167H/R167H}$ or the $TP53^{R167H/+}$ pigs (Sieren *et al.*, 2014a). Necropsy of one of the silica exposed pigs confirmed persistent silica deposition in the lung and localized fibrosis development. The remaining animals continue to be monitored for further disease progression.

As sufficient data from this longitudinal project is collected, we will then be able to evaluate our imaging data and correlate this to macroscopic and microscopic pathological changes. The application of imaging to correlate with pathological changes has been described (Tempel-Brami et al., 2015) and has been employed to study small animal models such as mice (Ramot et al, 2014) and large animal models such as pigs (Sieren et al., 2014a, Hariri et al 2013). The longitudinal imaging and analysis methods presented in this paper will be vital in the continued development and exploration of this pig model, including further histopathological confirmation of identified disease.

In conclusion, in this study we have developed optimized CT and MRI imaging and reporting methods for longitudinal lung studies of the pig silica exposure model. We developed structured reporting approaches for standardizing radiologist interpretation and quantitatively cross-comparing CT and MRI modality performance for the detection of pulmonary structural changes indicative of disease. The integration of these methods

provides a procedure and valuable multi-modality cross-comparison for refinement of protocols developed for characterization of other pig models and consistently monitors potential areas of interest for guided biopsy and/or necropsy.

Acknowledgments

This research was supported in part by the NIH (UL1 TR000442, P30 ES005605, and R01HL112986) along with in kind support from Exemplar Genetics. We thank Christopher Rogers, Frank Rohret, Judy Rohret, Jason Struzynski, Tony Smith, David Stoltz, Mahmoud Abou, Mark Hoegger, Chelsea Sloan, Melissa Shirk, Elizabeth Allard, Marla Kleingartner, Autumn Craig, Peter Thorne, and Andrea Dodd for technical assistance.

Abbreviations

CT	Computed Tomography
CTDIvol	Computed Tomography Dose Index Volume
HU	Hounsfield Units
MRI	Magnetic Resonance Imaging
PEEP	Positive End Expiratory Pressure
ET-CO_2	End-Tidal Carbon Dioxide pressure
SpO_2	Peripheral capillary oxygen saturation
VIBE	Volume Interpolated Breath-hold Examination (Fast 3D Gradient Echo MRI Pulse Sequence)
T1	Spin-lattice relaxation time
T2	Spin-spin relaxation time
RSNA	Radiologic Society of North America
TE	Echo Time
TR	Repetition Time
ROI	Region of Interest
IACUC	Institutional Animal Care and Use Committee
AAALAC	Association for Assessment and Accreditation of Laboratory Animal Care
kVp	kilovolts peak
mAs	milliamp-seconds

References

Alford SK, van Beek EJ, McLennan G, Hoffman EA. Heterogeneity of pulmonary perfusion as a mechanistic image-based phenotype in emphysema susceptible smokers. Proceedings of the National Academy of Sciences. 2010; 107:7485–7490.

Bell LC, Johnson KM, Fain SB, Wentland A, Drees R, Johnson RA, Bauman G, Francois CJ, Nagle SK. Simultaneous MRI of lung structure and perfusion in a single breathhold. J Magn Reson Imaging. 2015; 41:52–59. [PubMed: 24357054]

Bode G, Clausing P, Gervais F, Loegsted J, Luft J, Nogues V, Sims J. The utility of the minipig as an animal model in regulatory toxicology. J Pharmacol Toxicol Methods. 2010; 62:196–220. [PubMed: 20685310]

Checkoway H, Hughes JM, Weill H, Seixas NS, Demers PA. Crystalline silica exposure, radiological silicosis, and lung cancer mortality in diatomaceous earth industry workers. Thorax. 1999; 54:56–59. [PubMed: 10343633]

Cherry NM, Burgess GL, Turner S, McDonald JC. Crystalline silica and risk of lung cancer in the potteries. Occup Environ Med. 1998; 55:779–785. [PubMed: 9924456]

Couch MJ, Ball IK, Li T, Fox MS, Ouriadov AV, Biman B, Albert MS. Inert fluorinated gas MRI: a new pulmonary imaging modality. NMR Biomed. 2014; 27:1525–1534. [PubMed: 25066661]

Dakin JH, Evans TW, Hansell DM, Hoffman EA. Regional pulmonary blood flow in humans and dogs by 4D computed tomography. Acad Radiol. 2008; 15:844–852. [PubMed: 18572119]

Ellinwood NM, Clay CM. Large animal models of genetic disease: pertinent IACUC issues. ILAR journal / National Research Council, Institute of Laboratory Animal Resources. 2009; 50:225–228.

Fain SB, Korosec FR, Holmes JH, O'Halloran R, Sorkness RL, Grist TM. Functional lung imaging using hyperpolarized gas MRI. J Magn Reson Imaging. 2007; 25:910–923. [PubMed: 17410561]

Ganz SD. Presurgical planning with CT-derived fabrication of surgical guides. J Oral Maxillofac Surg. 2005; 63:59–71. [PubMed: 16125016]

Guo, J.; Fuld, M.; Alford, S.; Reinhardt, J.; Hoffman, E. Pulmonary Analysis Software Suite 9.0: Integrating quantitative measures of function with structural analyses. Proceedings of the First International Workshop on Pulmonary Image Analysis; 2008. p. 283-292.

Hammond E, Dilger SK, Stoyles N, Judisch A, Morgan J, Sieren JC. Consistent and reproducible positioning in longitudinal imaging for phenotyping genetically modified swine. SPIE Medical Imaging. 2015; 9417:941729-1–941729-7.

Hariri LP, Applegate MB, Mino-Kenudson M, Mark EJ, Bouma BE, Tearney GJ, Suter MJ. Optical frequency domain imaging of ex vivo pulmonary resection specimens: obtaining one to one image to histopathology correlation. Journal of visualized experiments : JoVE. 2013

Henne E, Ferguson JS, Mest R, Herth FJ. Thermal Vapor Ablation for Lung Lesions in a Porcine Model. Respiration. 2015; 90:146–154. [PubMed: 26160498]

Johnson KM, Fain SB, Schiebler ML, Nagle S. Optimized 3D ultrashort echo time pulmonary MRI. Magn Reson Med. 2013; 70:1241–1250. [PubMed: 23213020]

Kahn CE Jr, Langlotz CP, Burnside ES, Carrino JA, Channin DS, Hovsepian DM, Rubin DL. Toward Best Practices in Radiology Reporting 1. Radiology. 2009; 252:852–856. [PubMed: 19717755]

Kotoulas C, Panagiotou I, Tsipas P, Melachrinou M, Alexopoulos D, Dougenis D. Experimental studies in the bronchial circulation. Which is the ideal animal model? J Thorac Dis. 2014; 6:1506–1512. [PubMed: 25364530]

Levine AJ, Oren M. The first 30 years of p53: growing ever more complex. Nature Reviews Cancer. 2009; 9:749–758.

Matsumoto S, Mori H, Miyake H, Yamada Y, Ueda S, Oga M, Takeoka H, Anan K. MRI signal characteristics of progressive massive fibrosis in silicosis. Clin Radiol. 1998; 53:510–514. [PubMed: 9714391]

Mobberley SD, Fuld MK, Sieren JP, Primak AN, Hoffman EA. Scatter Correction Associated with Dedicated Dual-source CT Hardware Improves Accuracy of Lung Air Measures. Acad Radiol. 2013; 20:1334–1343. [PubMed: 24119345]

Mosiewicz J, Myslinski W, Zlomaniec G, Czabak-Garbacz R, Krupski W, Dzida G. Diagnostic value of high resolution computed tomography in the assessment of nodular changes in pneumoconiosis in foundry workers in Lublin. Ann Agric Environ Med. 2004; 11:279–284. [PubMed: 15627337]

Muhle H, Kittel B, Ernst H, Mohr U, Mermelstein R. Neoplastic lung lesions in rat after chronic exposure to crystalline silica. Scand J Work Environ Health. 1995; 21(Suppl 2):27–29. [PubMed: 8929684]

O'Connell DP, Thomas DH, Dou TH, Lamb JM, Feingold F, Low DA, Fuld MK, Sieren JP, Sloan CM, Shirk MA, Hoffman EA, Hofmann C. Comparison of breathing gated CT images generated using a 5DCT technique and a commercial clinical protocol in a porcine model. Medical Physics. 2015; 42:4033–4042. [PubMed: 26133604]

Ramot Y, Brauner R, Kang K, Heymach JV, Furtado S, Nyska A. Quantitative evaluation of drug-induced microvascular constriction in mice kidney using a novel tool for 3D geometrical analysis of ex vivo organ vasculature. Toxicol Pathol. 2014; 42:774–783. [PubMed: 24670814]

Rice F, Park R, Stayner L, Smith R, Gilbert S, Checkoway H. Crystalline silica exposure and lung cancer mortality in diatomaceous earth industry workers: a quantitative risk assessment. Occup Environ Med. 2001; 58:38–45. [PubMed: 11119633]

Rogers CS, Abraham WM, Brogden KA, Engelhardt JF, Fisher JT, McCray PB, McLennan G, Meyerholz DK, Namati E, Ostedgaard LS. The porcine lung as a potential model for cystic fibrosis. American Journal of Physiology-Lung Cellular and Molecular Physiology. 2008a; 295:L240–L263. [PubMed: 18487356]

Rogers CS, Stoltz DA, Meyerholz DK, Ostedgaard LS, Rokhlina T, Taft PJ, Rogan MP, Pezzulo AA, Karp PH, Itani OA, Kabel AC, Wohlford-Lenane CL, Davis GJ, Hanfland RA, Smith TL, Samuel M, Wax D, Murphy CN, Rieke A, Whitworth K, Uc A, Starner TD, Brogden KA, Shilyansky J, McCray PB, Zabner J, Prather RS, Welsh MJ. Disruption of the CFTR Gene Produces a Model of Cystic Fibrosis in Newborn Pigs. Science. 2008b; 321:1837–1841. [PubMed: 18818360]

Saffiotti U. Lung cancer induction by crystalline silica. Prog Clin Biol Res. 1991; 374:51–69. [PubMed: 1320275]

Sieren JC, Meyerholz DK, Wang XJ, Davis BT, Newell JD Jr, Hammond E, Rohret JA, Rohret FA, Struzynski JT, Goeken JA, Naumann PW, Leidinger MR, Taghiyev A, Van Rheeden R, Hagen J, Darbro BW, Quelle DE, Rogers CS. Development and translational imaging of a TP53 porcine tumorigenesis model. The Journal of Clinical Investigation. 2014a; 124:4052–4066. [PubMed: 25105366]

Sieren JP, Hoffman EA, Fuld MK, Chan KS, Guo J, Newell JD. Sinogram Affirmed Iterative Reconstruction (SAFIRE) versus weighted filtered back projection (WFBP) effects on quantitative measure in the COPDGene 2 test object. Medical Physics. 2014b; 41:091910. [PubMed: 25186397]

Svendsen O. The minipig in toxicology. Exp Toxicol Pathol. 2006; 57:335–339. [PubMed: 16725317]

Swindle M, Makin A, Herron A, Clubb F, Frazier K. Swine as models in biomedical research and toxicology testing. Vet Pathol. 2012; 49:344–356. [PubMed: 21441112]

Tan KM, Shishkov M, Chee A, Applegate MB, Bouma BE, Suter MJ. Flexible transbronchial optical frequency domain imaging smart needle for biopsy guidance. Biomed Opt Express. 2012; 3:1947–1954. [PubMed: 22876357]

Tempel-Brami C, Schiffenbauer YS, Nyska A, Ezov N, Spector I, Abramovitch R, Maronpot RR. Practical Applications of in Vivo and ex Vivo MRI in Toxicologic Pathology Using a Novel High-performance Compact MRI System. Toxicol Pathol. 2015; 43:633–650. [PubMed: 25694086]

Won C, Chon D, Tajik J, Tran BQ, Robinswood GB, Beck KC, Hoffman EA. CT-based assessment of regional pulmonary microvascular blood flow parameters. J Appl Physiol. 2003; 94:2483–2493. [PubMed: 12588787]

Zach JA, Newell JD Jr, Schroeder J, Murphy JR, Curran-Everett D, Hoffman EA, Westgate PM, Han MK, Silverman EK, Crapo JD, Lynch DA. Quantitative computed tomography of the lungs and airways in healthy nonsmoking adults. Invest Radiol. 2012; 47:596–602. [PubMed: 22836310]

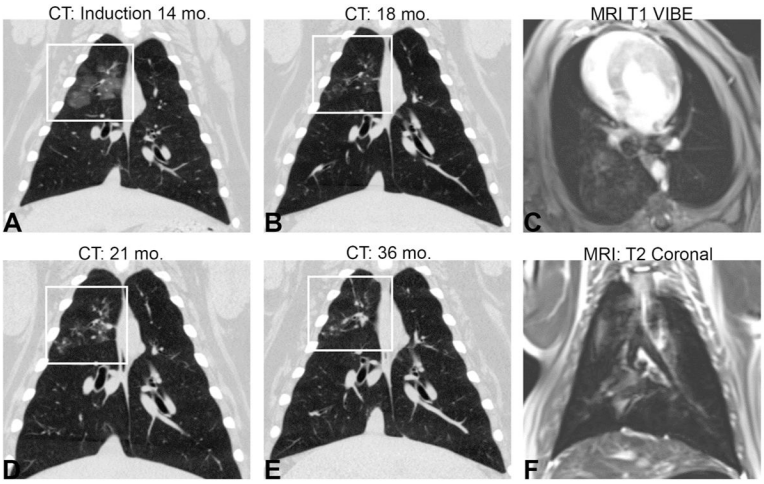

Figure 1. Longitudinal development of disease and lung images

The progression of disease, highlighted by the white box, in subject 4 from (A) deposition of silica at 14 months and disease progression at (B) 16 months, (C) 21 months, and (D) 36 months of age. Example MRI images from subject 3 at 18 months (E) post-contrast T1-weighted scan VIBE and (F) turbo spin echo T2-weighted scan.

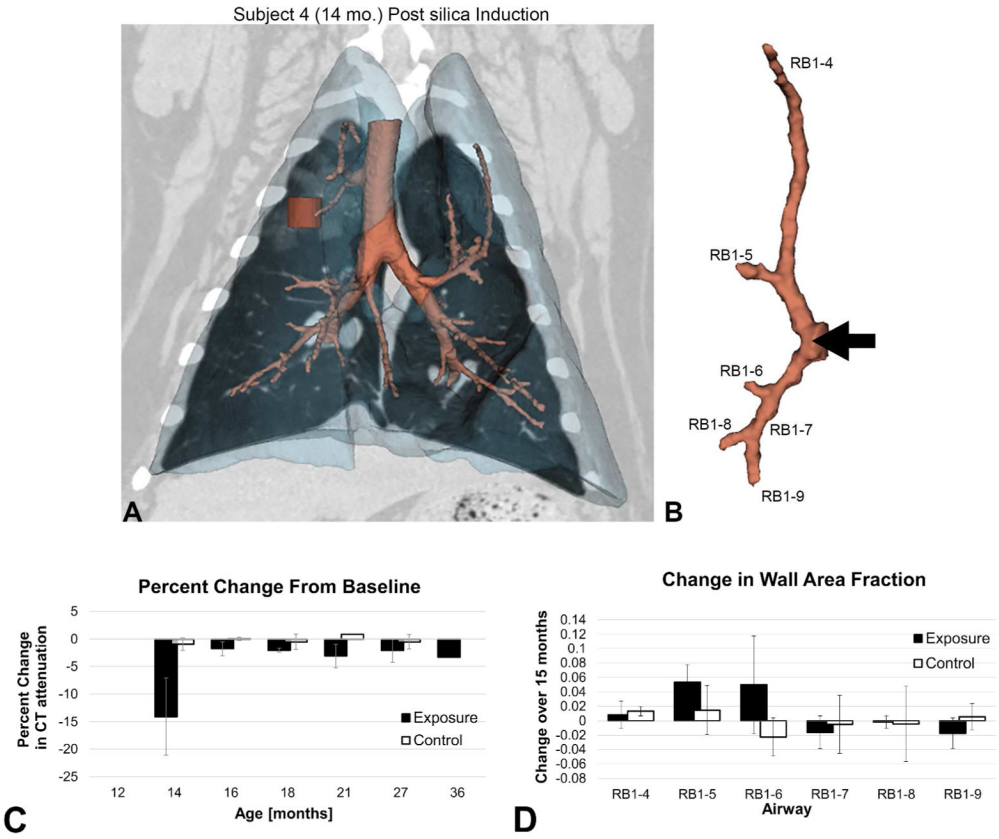

Figure 2. Silica deposition and corresponding quantitative measures

(A) Volumetric rendering of the lungs (translucent blue) with the corresponding airway tree (peach) from subject 4. The red cylinder within the upper lung indicates the location of the volumetric region of interest (ROI) used for CT attenuation analysis. The corresponding CT coronal-section shows the deposition of silica as noted by the increased attenuation in the surrounding area. (B) The apical bronchus airway tree and the labeling system used to identify each branch. The black arrow shows the site of silica deposition with the bronchoscope corresponding to the black arrow in A. (C) Percent change from baseline (at 12 months of age) of lung attenuation (measured in Hounsfield Units) in the ROI for exposure and control animals. Due to the nature of CT in the lungs (negative Hounsfield Unit values), an increase in attenuation results in a negative percent change. (D) Change in wall area fraction in the peripheral airways of the apical bronchus tree. Change is determined as the difference between wall area fraction measures at 15 months post exposure (27 months of age) versus those acquired at baseline (12 months of age).

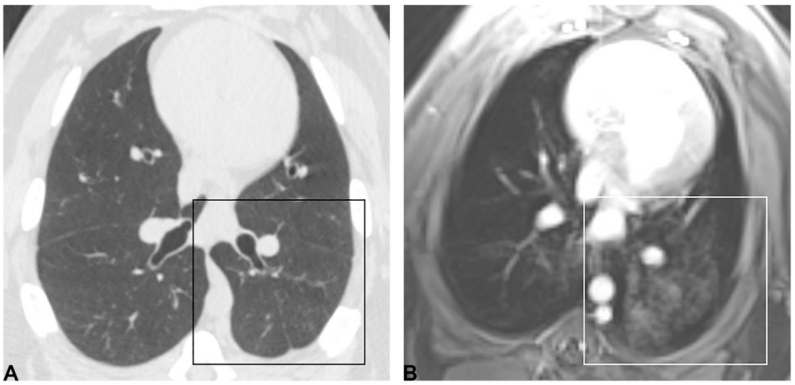

Figure 3. Ground glass artifact in MRI thoracic scan

The high detection of ground glass in the (B) MRI datasets in the upper lung compared to the low detection of ground class in the corresponding (A) CT images indicated the presence of an artifact in the T1 post-contrast images as indicated by the boxes. Image data from Subject 6 at 18 months.

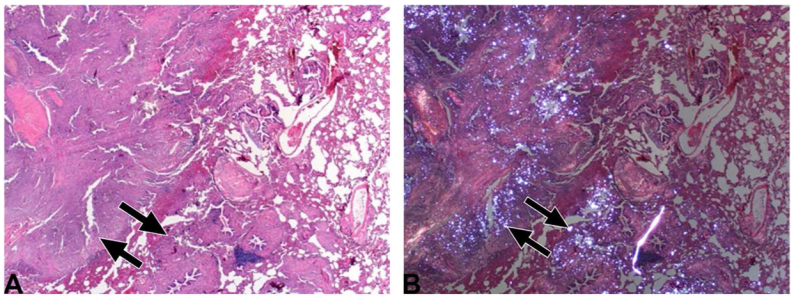

Figure 4. Pathological confirmation of silica deposits and disease development

(A) Histopathological appearance of the lung (from Subject 4, see also Figure 1D) showed locally extensive remodeling accentuated by fibrosis (arrows) and inflammation (HE stain, 20x). (B) Same section as Figure 4A, but examined with polarized light. Note that the white (refractile) silica granules (arrows) are admixed within pulmonary remodeling (HE stain, 20x).

Table 1

Subjects and screening time points

X indicates that imaging occurred, S indicates that silica was injected with corresponding imaging occurring, and N indicates that necropsy was performed following imaging. The first 4 time points were used to compare the relative merits of the two imaging modalities. The remaining subjects continue to be monitored for progression.

		Age [mo.]																
Subjects		**11**	**12**	**13**	**14**	**15**	**16**	**17**	**18**	**19**	**20**	**21**	**22**	**26**	**27**	**28**	**35**	**36**
Control	2		X		X		X		X			X			X			
	5		X		X		X		X						X			
	6		X		X		X		X						X			
Exposure	1		X		**S**		X		X			X			X			
	3		X		**S**		X		X			X			X			
	4		X		**S**		X		X			X			X			**N**

Table 2

Percent agreement between CT and MRI

Additional conditions included nodules, emphysema, cysts, reticular abnormalities and honeycombing, but were minimally identified. Percent agreement was calculated as the number of congruent findings (presence and absence of condition) divided by the total number of time points.

Lobe	Right cranial	Right middle	Right lower	Accessory	Left Cranial	Left Lower	Total
Consolidation	78%	87%	83%	100%	100%	48%	83%
Bronchiectasis	74%	83%	48%	96%	96%	52%	75%
Atelectasis	74%	78%	91%	96%	70%	78%	81%
Bronchial wall thickening	91%	100%	70%	100%	96%	83%	90%
Ground glass opacities	30%	96%	39%	100%	35%	30%	55%
Linear opacities	52%	52%	17%	96%	52%	17%	48%
Total	67%	83%	58%	98%	75%	51%	**72%**